nature medicine

miR-141 and miR-200a act on ovarian tumorigenesis by controlling oxidative stress response

Bogdan Mateescu[1,2], Luciana Batista[1,2], Melissa Cardon[1,2], Tina Gruosso[1,2], Yvan de Feraudy[1,2], Odette Mariani[3], André Nicolas[3], Jean-Philippe Meyniel[4], Paul Cottu[5], Xavier Sastre-Garau[3] & Fatima Mechta-Grigoriou[1,2]

Although there is evidence that redox regulation has an essential role in malignancies, its impact on tumor prognosis remains unclear. Here we show crosstalk between oxidative stress and the miR-200 family of microRNAs that affects tumorigenesis and chemosensitivity. miR-141 and miR-200a target p38α and modulate the oxidative stress response. Enhanced expression of these microRNAs mimics p38α deficiency and increases tumor growth in mouse models, but it also improves the response to chemotherapeutic agents. High-grade human ovarian adenocarcinomas that accumulate miR-200a have low concentrations of p38α and an associated oxidative stress signature. The miR200a-dependent stress signature correlates with improved survival of patients in response to treatment. Therefore, the role of miR-200a in stress could be a predictive marker for clinical outcome in ovarian cancer. In addition, although oxidative stress promotes tumor growth, it also sensitizes tumors to treatment, which could account for the limited success of antioxidants in clinical trials.

Epithelial ovarian cancer is the most lethal form of gynecologic malignancy. The clinical prognosis factors for this type of cancer are based on the state of the disease at diagnosis, including histological subtype, grade, stage and extent of residual disease after surgery. Despite the use of treatment strategies that combine surgery and chemotherapy, patients with epithelial ovarian cancer often relapse and eventually die from their disease[1]. In recent years, several studies have analyzed large-scale transcription profiling to identify differentially expressed genes according to tumor status, histological subtypes and metastatic spread[2]. However, the molecular biology of ovarian cancer is still not completely understood, making the development of more effective therapies difficult. Therefore, there is a pressing need to explore the biological basis of ovarian cancer to search for early diagnostic classifiers that can reliably stratify patients for therapeutic intervention.

Accumulation of reactive oxygen species (ROS) in tumor cells damages their cellular components and alters various processes, including gene expression, proliferation and genomic stability[3–9]. Of the many adaptive mechanisms that modulate gene expression in response to stress, the p38α mitogen-activated protein kinase (MAPK) family acts as a sensor of oxidative stress, and its redox-sensing function is essential in the control of tumor development[10,11]. In contrast to other MAPKs such as extracellular signal-regulated kinase (ERK) or cJun NH2-terminal kinase (JNK), which can promote either proliferation or survival, p38α often suppresses tumorigenesis by blocking proliferation or promoting apoptosis[12–15]. In addition, miRNA expression can be altered by distinct stress conditions such as radiation, oxidative stress or hypoxia[16–21]. In this regard, miRNAs are essential regulators of the stress response across multiple species.

Here we identify a new function for the miR-200 family members (miR-200s) in oxidative stress and ovarian tumorigenesis. These miRNAs were previously shown to modulate cellular motility and control 'stemness' and apoptosis[22–33]. We now show that two members of the miR-200 family (miR-141 and miR-200a) inhibit p38α and have an essential role in redox sensing. In mouse models, accumulation of these miRNAs mimics p38α deficiency and promotes malignancy. Human ovarian adenocarcinomas characterized by high miR-200a expression show low amounts of p38α protein and have an associated oxidative stress signature. Notably, this signature is correlated with longer progression-free survival (PFS) and overall survival. Consistent with these findings, although overexpression of miR-200a or miR-141 promotes tumorigenesis under untreated conditions, it increases tumor-cell death and slows tumor growth under treatment with paclitaxel, a chemotherapeutic drug known to increase ROS[34–36]. Thus, the miR-200–dependent stress response could have a dual function in tumors: although this response increases tumor growth, it could also enhance sensitivity to chemotherapy. In addition, we identify a new function for miR-200s in the stress response, which could be a predictive marker for clinical outcome in ovarian cancers.

RESULTS

Expression of miR-200s is stimulated by oxidative stress

Using a microarray analysis, we identified a set of 36 miRNAs whose expression was changed after exposure of fibroblasts to acute oxidative stress (**Fig. 1a**). Twenty of these miRNAs were upregulated and 16 were downregulated by H_2O_2 treatment over time. In particular, the expression of the miR-200s was stimulated by oxidative stress (**Fig. 1a**,**b**).

[1]Stress and Cancer Laboratory, Institut Curie, Paris, France. [2]Institut National de la Santé et de la Recherche Médicale, U830, Paris, France. [3]Institut Curie, Department of Pathology, Paris, France. [4]Institut Curie, Functional Genomic Platform, Paris, France. [5]Institut Curie, Department of Medical Oncology, Paris, France. Correspondence should be addressed to F.M.-G. (fatima.mechta-grigoriou@curie.fr).

Received 12 January; accepted 14 September; published online 20 November 2011; doi:10.1038/nm.2512

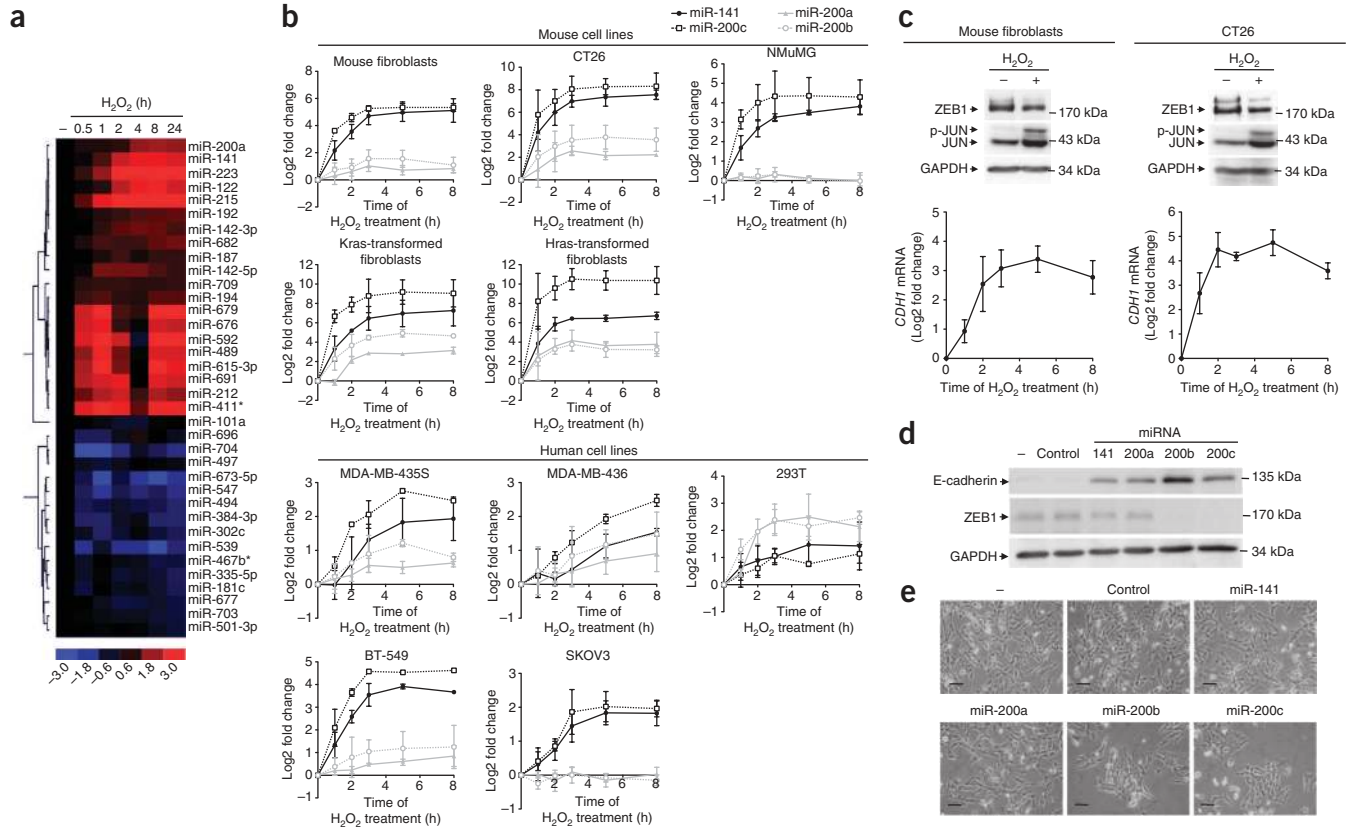

Figure 1 Expression of the miR-200s is stimulated by oxidative stress. (**a**) Unsupervised hierarchical clustering of miRNA microarray expression data from mouse fibroblasts after exposure to H_2O_2 for various durations. These miRNAs were selected on the basis of their differential expression ($P \leq 0.05$) at early (0.5–1 h), middle (2–4 h) or late (8–24 h) time points of treatment, when compared to untreated fibroblasts. The values shown are the means of the normalized expressions from two independent experiments. Upregulated and downregulated miRNAs after stress are shown in red and blue, respectively. (**b**) qRT-PCR of the miR-200s after a time course of H_2O_2 treatment in mouse cells (immortalized fibroblasts, colon carcinoma (CT26), mammary gland epithelial cells (NMuMG) and Kras- and Hras-transformed fibroblasts) and human cell lines (melanoma cells (MDA-MB-435S), kidney cells (293T), breast adenocarcinoma (MDA-MB-436 and BT-549) and ovarian adenocarcinoma (SKOV3)). Data are the means of fold changes (normalized to untreated and expressed as log2) ± s.d. (**c**) Top, western blot of ZEB1 protein in mouse fibroblasts and carcinoma cells (CT26) after 3 h of H_2O_2 exposure, at which point the miR-200s reached their maximum expression. Jun protein, its phosphorylated isoform (p-Jun) and glyceraldehyde-3-phosphate dehydrogenase (GAPDH) were used as internal controls for H_2O_2 treatment and protein loading, respectively. Bottom, E-cadherin mRNA levels in fibroblasts and CT26 cells after H_2O_2 exposure are shown. (**d**,**e**) Shown are the amounts of E-cadherin and ZEB1 protein (**d**) and the cellular morphology (**e**) in untransfected fibroblasts (–) or at 3 d after transfection with a control miRNA or the miR-200s. All transfected miRNAs are expressed to the same range (with a qRT-PCR cycle threshold (C_t) of 13.4 ± 0.7 C_t on average). Scale bars, 15 μm. All experiments were performed in triplicate, and error bars represent means ± s.e.m. (unless otherwise specified) from at least three independent experiments.

miRNAs from each locus (**Supplementary Fig. 1a**,**b**) had the same kinetics after induction by stress (**Fig. 1b**). Overall, expression of the miR-200s was induced within 1 h of treatment, reached its maximum between 2 and 3 h after treatment and was maintained at later time points. The miR-200s were upregulated with similar kinetics in fibroblasts and epithelial cells from mouse and human (**Fig. 1b**). In cell lines already expressing high basal concentrations of the miR-200s, we did not detect upregulation (**Supplementary Fig. 1c**,**d**). Upregulation of the miR-200s was specific to H_2O_2 exposure, and we did not observe upregulation with other stimuli or stressors (**Supplementary Fig. 1e**), further showing these miRNAs might be involved in response to oxidative stress.

The miR-200s have been shown to regulate the mesenchymal-to-epithelial transition (MET) through modulation of the E-cadherin transcriptional repressor zinc finger E-box binding homeobox 1 (ZEB1)[22–27,32,33]. Accordingly, treatment of fibroblasts or colon carcinoma cells with H_2O_2 reduced the amount of ZEB1 protein and enhanced E-cadherin transcription but was not sufficient to induce a stable MET, as H_2O_2 hydrolysis prevented long-lasting miR-200 accumulation (**Fig. 1c**, **Supplementary Fig. 1f** and **data not shown**). This suggests that the regulation of miR-200s by stress, among other mechanisms, could be involved in the control of E-cadherin expression. When overexpressed in fibroblasts, the miR-200s stabilized E-cadherin expression by targeting its transcriptional repressor, ZEB1 (**Fig. 1d**). Although all the miR-200s were overexpressed to the same extent, stabilization of E-cadherin was more efficient when miR-200b or miR-200c was overexpressed than when miR-141 or miR-200a was overexpressed. Accordingly, we detected miRNA-induced clustering of epithelial cells only with miR-200b or miR-200c and not with miR-141 or miR-200a (**Fig. 1e**). This further suggests that the miR-200s have different cellular functions, which led us to investigate their specific role in the oxidative stress response.

miR-141 and miR-200a inhibit p38α

To determine the function of miR-200 in oxidative stress, we compared the ROS-dependent signaling pathway of cells overexpressing miR-141 or miR-200a to cells overexpressing a control miRNA when exposed to

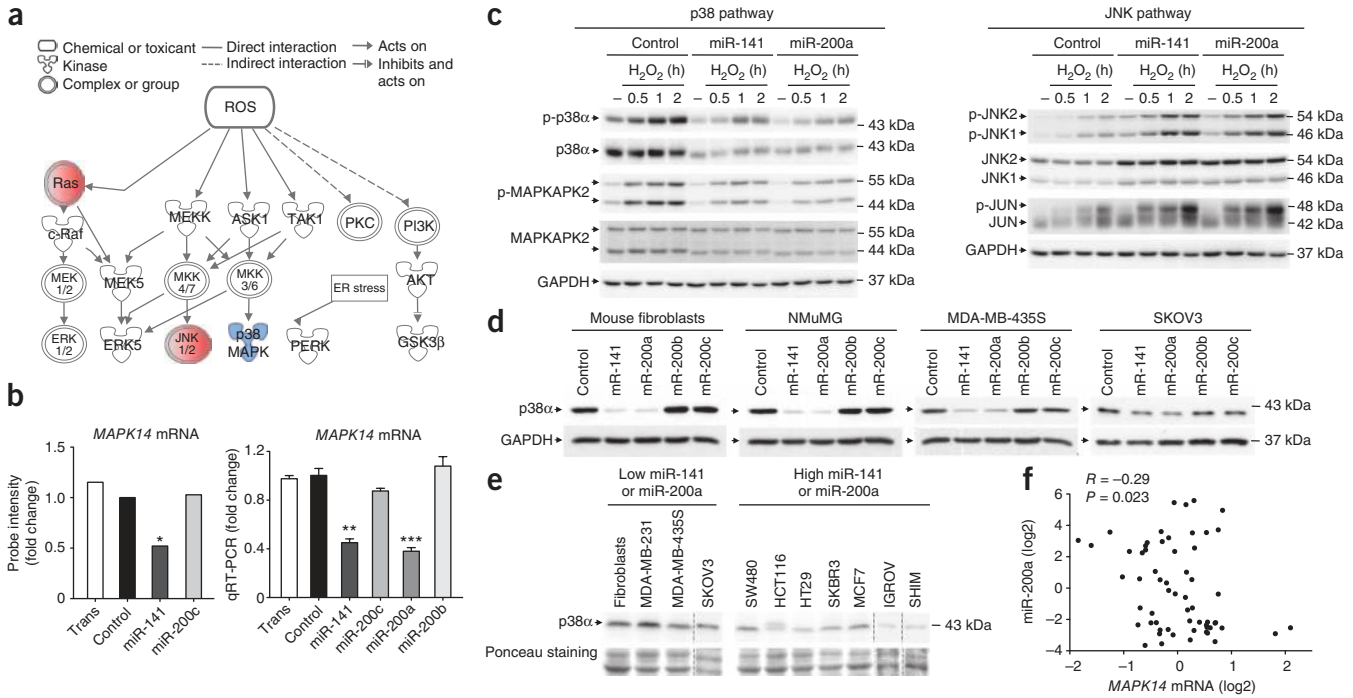

Figure 2 Balance of the p38 and JNK pathways by miR-141 and miR-200a. (**a**) Scheme of the ROS signaling pathway showing mRNAs affected by mir-141 overexpression in mouse fibroblasts stimulated by H_2O_2. Significantly upregulated and downregulated mRNAs are shown in red and blue, respectively ($P \leq 0.05$). The fold changes are normalized to cells overexpressing control miRNA. (**b**) *MAPK14* mRNA level evaluated by microarray (left) or qRT-PCR (right) in mouse fibroblasts 3 d after transfection with a transfection reagent (trans), control miRNA (control) or a specific miRNA, as indicated. Data are the means of fold changes (normalized to control) ± s.e.m. $^*P \leq 0.05$, $^{**}P \leq 0.01$, $^{***}P \leq 0.001$ by Student's *t* test. (**c**) Western blots showing MAPK-related proteins in mouse fibroblasts transfected with specific miRNA, as noted, under basal conditions (–) or after H_2O_2 exposure. P-, phospho-. (**d**) Western blots showing the amount of p38α protein in mouse (fibroblasts and NMuMG) and human (MDA-MB-435S and SKOV3) cell lines after miRNA transfection. (**e**) Western blot showing the amount of p38α protein in diverse human cancer cell lines. A cell line belongs to the 'high' class of miR-141 or miR-200a if at least one of these mRNA's content is above the average miR-141 or miR-200a level from all the analyzed cell lines; a cell line belongs to the 'low' class if both miR-141 and miR-200a content is below the average. Using this rule, cells belonging to the 'high miR-141 or miR-200a' class express at least one of the miRNAs at a fivefold higher level than their average levels. (**f**) Correlation plot extracted from NCI60 microarray data sets showing that *MAPK14* mRNA level is inversely correlated with endogenous miR-200a levels ($R = -0.29$, $P = 0.023$ by Pearson's test).

H_2O_2. Microarray experiments and further analyses using Ingenuity Pathway Analysis (IPA) software indicated that miR-141 or miR-200a altered MAPK response to H_2O_2 by modulating the p38α and JNK pathways (**Fig. 2a**). Indeed, expression of mitogen-activated protein kinase 14 (*Mapk14*) (encoding p38α) was significantly downregulated by miR-141 or miR-200a overexpression, as evaluated by microarrays and confirmed by quantitative RT-PCR (qRT-PCR) (**Fig. 2b**). The expression of *Mapk14* was unchanged by overexpression of miR-200c or miR-200b (**Fig. 2b**), suggesting that only miR-141 and miR-200a are involved in the regulation of the MAPK pathway.

miR-141 and miR-200a have high sequence homology (**Supplementary Fig. 1a**), suggesting they target the same proteins. Overexpression of miR-141 or miR-200a severely reduced the total amount of p38α protein under either basal or stressed conditions (**Fig. 2c** and **Supplementary Fig. 2b**). This reduction prevented the expected accumulation of the phosphorylated form of p38α and led to the subsequent decreased phosphorylation of MAPK-activated protein kinase 2 (MAPKAPK2), one of the major downstream effectors of p38α (**Fig. 2c**). Furthermore, overexpression of miR-141 or miR-200a was associated with the constitutive activation of the JNK pathway (**Fig. 2c**), as was previously seen after *Mapk14* inactivation[12]. In cells expressing miR-141 or miR-200a, as in $Mapk14^{-/-}$ cells, we observed an earlier and higher phosphorylation rate of JNK1, JNK2 and JNK targets, for example, the proto-oncogene Jun (**Fig. 2c**). We confirmed that overexpression of miR-141 or miR-200a led to p38α downregulation in various mouse and human cell lines, whereas overexpression of miR-200c or miR-200b had no effect (**Fig. 2d**). These results indicate specific control of p38α by miR-141 or miR-200a in the basal state or under stressed conditions in human and mouse cells. Accordingly, cell lines with high endogenous concentrations of miR-141 or miR-200a had lower amounts of p38α protein than those lines characterized by low expression of miR-141 or miR-200a (**Fig. 2e**). The *MAPK14* mRNA level was significantly inversely correlated with miR-200a expression (**Fig. 2f**) when evaluated using the US National Cancer Institute's NCI60 database, which contains a panel of 60 diverse human cancer cell lines[37]. In addition, miR-200a was the sixth-ranked miRNA among 422 miRNAs with respect to an inverse correlation with *MAPK14*. Reciprocally, *MAPK14* was ranked 3,616th among the 41,078 probe sets for miR-200a. Finally, we found that the 3′ untranslated region of *MAPK14* was directly targeted by miR-141 or miR-200a, and we identified the genuine binding site of these miRNAs in humans and mice (**Supplementary Fig. 3**). These data show that miR-141 and miR-200a are key direct regulators of p38α.

miR-141 and miR-200a promote tumorigenesis in mouse models

Because miR-141 and miR-200a have homologous sequences, we tested whether the downregulation of p38α by miRNA could affect

transformation in Kras-transformed fibroblasts overexpressing miR-141. We confirmed the accumulation of miR-141 in these stable clones (**Supplementary Fig. 4a**). When plated in soft agar, cells overexpressing miR-141 showed a markedly enhanced plating efficiency and growth rate compared to controls (**Fig. 3a**), indicating that miR-141 facilitates cell growth without substrate attachment. In addition, overexpression of miR-141 significantly increased the tumor size in xenografted nude mice (**Fig. 3b**). Analyzed when they reached the same size, tumors overexpressing miR-141 had a lower amount of p38α protein than control tumors (**Fig. 3c**). Furthermore, these tumors had a higher mitotic index and a greater number of large blood vessels compared to controls (**Fig. 3c**), as was previously shown for p38α-deficient tumors in a Ras-dependent context[10].

Because we detected marked effects for miR-141 and miR-200a in human ovarian carcinomas (see below), we assessed their effect on xenografted ovarian tumors. Ovarian cells stably overexpressing miR-141 or miR-200a (**Supplementary Fig. 4b**) gave rise to larger tumors when compared to control tumors (**Fig. 3d**). Tumors expressing miR-141 or miR-200a appeared earlier and grew faster than control tumors (**Fig. 3e**). Histological analyses confirmed that tumors overexpressing miR-141 or miR-200a had low amounts of p38α protein and were associated with a high mitotic index (**Fig. 3f**). Therefore, these data suggest that miRNA-dependent down-regulation of p38α has a positive role in tumorigenesis.

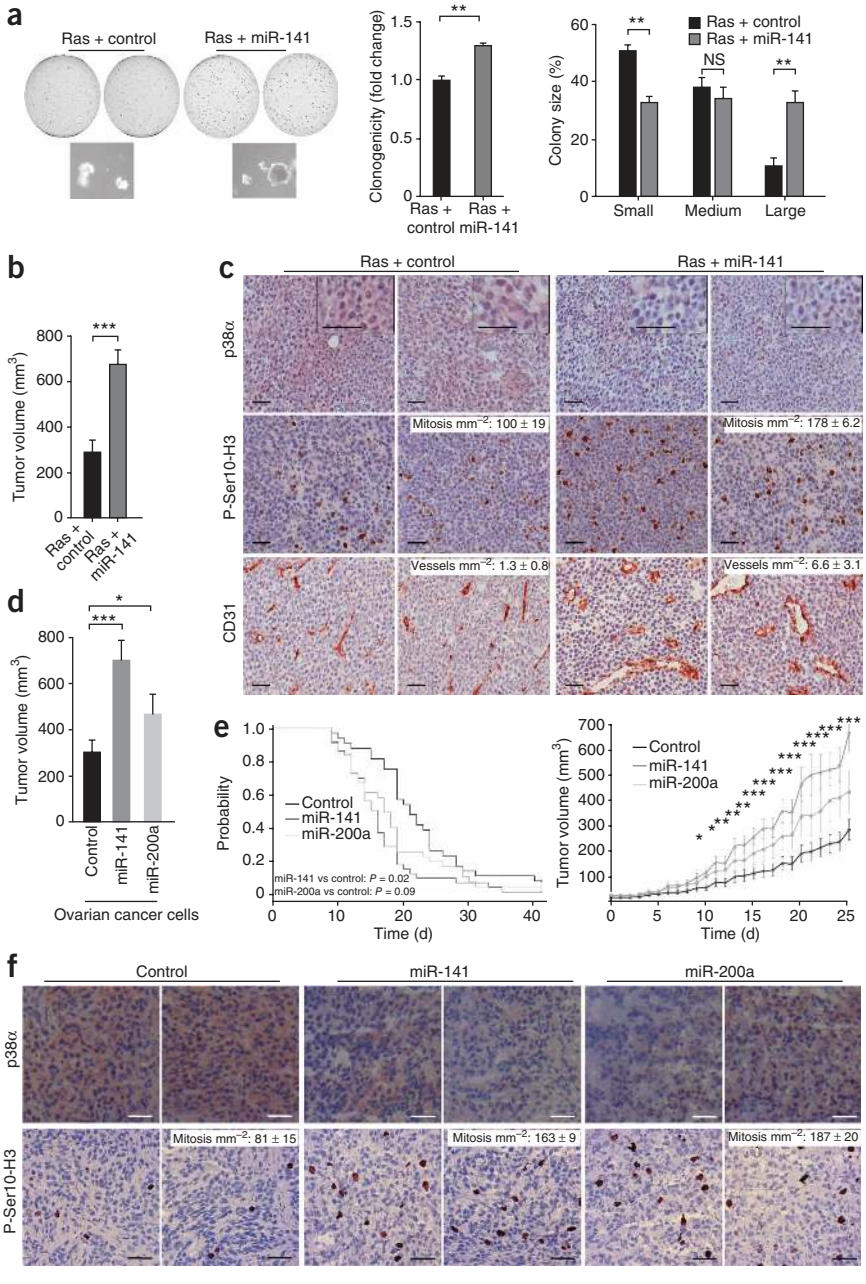

Figure 3 miR-141 and miR-200a enhance tumorigenesis in mouse models. (**a**) Left, representative dishes and individual colonies from Kras-transformed fibroblasts stably transfected with a control miRNA (Ras + control) or miR-141 (Ras + miR-141). Middle, relative number of visible colonies in soft agar formed from control and miR-141–overexpressing clones. Right, percentage of visible colonies arranged according to their size: small, ≤ 2.2 mm^2; 2.2 mm^2 < medium ≤ 4.5 mm^2; large, > 4.5 mm^2. Data are means ± s.e.m. (**b**) Tumor volumes 9 d after xenografting of control or miR-141–overexpressing Ras-transformed fibroblasts. Values are means ± s.e.m. $n = 10$ in each group. (**c**) Representative immunohistochemistry of each type of tumor using specific antibodies. Indicated in each category are the numbers of mitotic cells per mm^2 (mm^{-2}) ($P = 0.032$ by Student's t test) and large (width >15 μm) blood vessels per mm^2 ($P = 0.039$ by Student's t test). (**d**) Tumor volumes 20 d after xenografting of control and miR-141– or miR-200a–overexpressing ovarian cancer cells. $n \geq 17$ in each group. (**e**) Left, Kaplan-Meir tumor-free survival curves from control and miR-141– or miR-200a–overexpressing mice (log-rank test). Right, tumor growth curves (Student's t test). Data are means ± s.e.m. (**f**) Representative immunohistochemistry of control and miR-141– or miR-200a–overexpressing ovarian tumors using specific antibodies. Indicated in each category are the numbers of mitotic cells per mm^2. Control compared to miR-141, $P = 0.0008$ and control compared to miR-200a, $P = 0.0017$ by Student's t test. $^*P \leq 0.05$, $^{**}P \leq 0.01$, $^{***}P \leq 0.001$. NS, not significant (Student's t test). Scale bars, 50 μm.

miR-200a controls p38α and stress response in ovarian cancers

Because the miR-200s have been shown to accumulate in aggressive human ovarian adenocarcinomas[38–44], we investigated whether p38α is a predictive marker for these tumors. We analyzed a large set of human ovarian adenocarcinomas that included mostly serous-subtype and high-grade tumors. Clinical details and subject information are given in **Supplementary Table 1** and **Supplementary Table 2**. We observed that there was no correlation between *MAPK14* mRNA level and the amount of p38α protein (**Fig. 4a** and **Supplementary Table 2**). Notably, the miR-200a expression rate was significantly inversely correlated with the amount of p38α protein (Spearman correlation coefficient (R) = −0.37, $P = 6 \times 10^{-3}$) (**Fig. 4b** and **Supplementary Table 3**). We observed this same tendency with miR-141, although

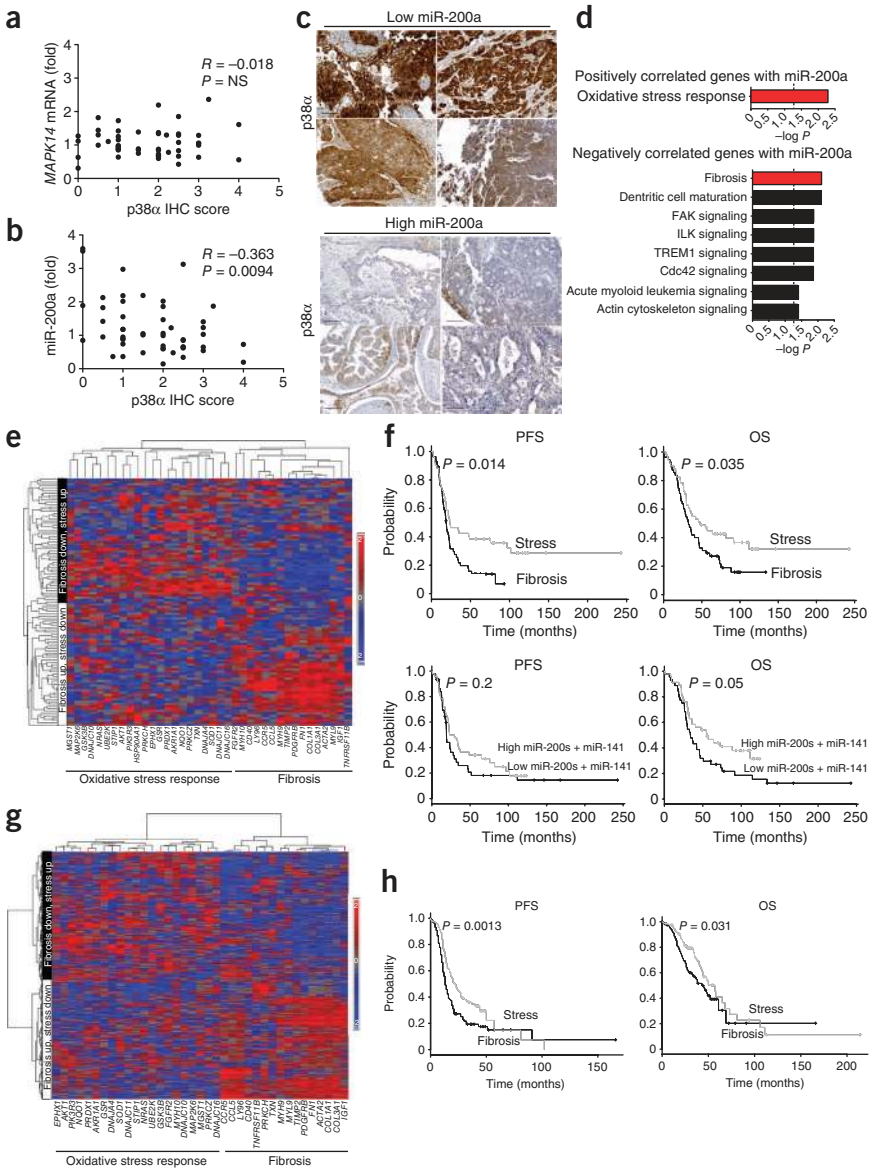

Figure 4 miR-200a and oxidative stress response predict good prognosis in patients with ovarian cancer. (**a**,**b**) Scatter diagrams showing the p38α immunohistochemistry (IHC) score relative to *MAPK14* mRNA (**a**) and miR-200a levels (**b**) in ovarian tumors (Spearman test). (**c**) Representative views of p38α immunostaining in tumors with low or high miRNA-200a levels. (**d**) Cellular pathways positively or negatively correlated with miR-200a levels in ovarian tumors. An unsupervised comparative analysis was done using a Fisher's exact test. *P* values were adjusted using a Benjamini-Hochberg multiple-testing correction. (**e**) An unsupervised hierarchical clustering of the stress and fibrosis signatures from the microarray ovarian cancer data set from the Institut Curie. Each row represents a tumor, and each column represents a gene. Red and blue indicate gene expression in a single tumor above and below the mean, respectively. The color saturation indicates the magnitude of the deviation from the mean. Genes cluster together according to the stress and fibrosis signatures (shown at the bottom of the matrix). The dendrogram of samples (on the left of the matrix) allows for the classification of subjects according to these signatures. Gene symbols and names are listed in **Supplementary Table 4**. (**f**) Kaplan-Meier curves of PFS and overall survival (OS) according to the two signatures ($n = 51$ for the stress signature, and $n = 56$ for the fibrosis signature) or to miR-200a or miR-141 expression ($n = 46$ for high expression and $n = 45$ for low expression). (**g**) Unsupervised hierarchical clustering of the signatures from the AOCS microarray data set. (**h**) Kaplan-Meier curves of PFS and overall survival of subjects from the AOCS data set according to the stress ($n = 158$) and fibrosis ($n = 128$) signatures. A log-rank test was used for the Kaplan-Meier curves. Scale bars, 50 μm.

the correlation was not significant ($R = -0.25$, $P = 0.07$). Tumors with high miR-200a expression showed faint p38α staining, and, conversely, tumors with low miR-200a expression showed bright p38α epithelial staining (**Fig. 4c**). Thus, in high-grade ovarian adenocarcinomas, regulation of p38α occurs, at least in part, in a miR-200a–dependent manner.

We next identified transcriptomic signatures associated with miR-200a in these tumors. Consistent with the function of miR-200 in MET, genes involved in MET-related pathways were significantly negatively correlated with miR-200a expression (**Fig. 4d** and **Supplementary Table 4**). Notably, the only relevant pathway significantly positively correlated with miR-200a expression was involved in oxidative stress response (**Fig. 4d** and **Supplementary Table 4**), indicating that the link between oxidative stress and miR-200a we uncovered *in vitro* is also relevant in a human-tumor context.

miR-200a-dependent signatures predict subject survival

We defined 'stress' and 'fibrosis' signatures by the genes that were positively and negatively correlated with miR-200a, respectively. The use of this dual signature allowed us to build a hierarchical cluster of ovarian tumors and to stratify subjects into two groups (**Fig. 4e**). Subjects classified as having the stress pattern (stress high, fibrosis low) had longer PFS and overall survival than those who had the fibrosis pattern (stress low, fibrosis high) (**Fig. 4f**). In contrast, using each single signature to stratify subjects did not allow to observe a differential in subject survival (data not shown), suggesting that both stress and fibrosis processes are required for fully recapitulating miR-200–dependent survival. Overall survival was significantly different according to the level of p38α-targeting miR-200s (miR-141 or miR-200a), and PFS tended toward the same observation (**Fig. 4f**). Notably, we validated the stress and fibrosis signatures in another set of individuals with ovarian cancer (from the Australian Ovarian Cancer Study (AOCS))[45] (**Fig. 4g**) and saw better prognoses for subjects with the stress pattern (**Fig. 4h**).

Although overexpression of miR-141 or miR-200a increased tumor growth in mice (**Fig. 3d**a–**f**), subjects with the stress pattern (high miR-200a expression) had better prognoses than subjects with the fibrosis pattern (low miR-200a expression) (**Fig. 4e**–**h**). This apparent paradox might be explained by different tumor aggressiveness or varying responses to treatment. We observed no correlation between signature and tumor grade (**Table 1**), probably because

Table 1 Characteristics of subjects and tumor samples associated with the stress and fibrosis signatures

		Grade			Stage				Debulking status		Biological response	Clinical response	
		1	2	3	I	II	III	IV	Optimal	Suboptimal	Log CA-125	Complete	Incomplete
Institut Curie	Stress	4	17	30	15	7	26	3	25	26	1.52 ± 0.10	28	14
	Fibrosis	3	17	36	6	3	33	14	13	43	1.92 ± 0.11	23	26
	P		NS			*P* = 0.004			*P* = 0.008		*P* = 0.010	*P* = 0.059	
AOCS	Stress	9	56	82	16	16	108	8	95	29			
	Fibrosis	10	41	82	8	2	109	14	65	41			
	P		NS			*P* = 0.002			*P* = 0.014				

Association of the stress and fibrosis signatures with clinical characteristics and remission status of patients in the Institut Curie and AOCS cohorts, when available. The biological response was evaluated by CA-125 after the first round of treatment. The clinical response was evaluated by the evolution of the mass of the tumor, determined by monitoring patients through their chemotherapeutic treatment; treatment was considered incomplete in patients with no or partial response to treatment. Debulking status was defined as optimal for tumor residues ≤1 cm in diameter after resection and as suboptimal for tumor residues >1 cm in diameter. Data are means of log values ± s.e.m. The *P* values were determined using χ^2 (for grade, stage and clinical response), Fischer exact (for debulking status) or Student's *t* (for CA-125) tests. NS, not significant.

there is a bias toward high-grade tumors in the cohorts from the Institut Curie and the AOCS (**Supplementary Table 1**). The fibrosis pattern was associated with partial debulking and high-stage tumors (**Table 1**). In addition, when considering tumor residual volume after the first round of treatment (as evaluated by plasma concentrations of cancer antigen 125, also called carbohydrate antigen 125, CA-125), we observed that the CA-125 concentrations were significantly lower in subjects with the stress pattern compared to those with the fibrosis pattern (**Table 1**). Similarly, physicians considered the clinical response, defined by variation in tumor mass after treatment, to be 'complete' (with significant reduction of tumor mass) in a large proportion of subjects with the stress pattern (**Table 1**). Finally, a multivariate analysis that included the miR-200a–dependent signatures (stress or fibrosis), age, tumor grade, histology and chemotherapy type showed that the signatures had an independent association with PFS (**Supplementary Table 5**). These observations suggest that the stress and fibrosis signatures defined by miR-200a may act on a patient's response to treatment.

We next investigated the effect of paclitaxel, a ROS-producing chemotherapeutic agent, on ovarian cancer cells overexpressing miRNA. Overexpression of miR-141 or miR-200a enhanced cell apoptosis after treatment with paclitaxel, whereas it protected cells against death in untreated conditions (**Fig. 5a**). As expected, the same results were obtained by inactivation of p38α (**Fig. 5a**). Moreover, we prevented the miR-141- and miR-200a–dependent effects on apoptosis by using antioxidants or inhibitors specific to miR-141 or miR-200a, further confirming the role of ROS, miR-141 and miR-200a in the sensitivity of cancer cells to paclitaxel (**Fig. 5a**). Notably, we observed similar effects *in vivo*. Whereas overexpression of miR-141 or miR-200a significantly increased tumor growth in untreated conditions (**Figs. 5b** and **3d–f**), mice with ovarian tumors overexpressing miR-141 or miR-200a were significantly more sensitive to paclitaxel than control mice (**Fig. 5b–d**). Therefore, expression of miR-141 or miR-200a promotes tumor growth but also increases sensitivity to chemotherapy. Our data prompted us to establish a proposed model, as described in **Figure 5e**.

DISCUSSION

Ovarian cancers are the most lethal gynecologic malignancies, and determining the molecular mechanisms involved in their development is a pressing need. The miR-200s were previously shown to accumulate in ovarian cancer[38–41,46,47]. Here we identify an miR-200a–dependent dual signature involved in oxidative stress and fibrosis that has predictive value. The fibrosis signature, defined by genes negatively correlated with miR-200a expression, corroborates its previously identified function on ZEB1 and ZEB2. Indeed, by inhibiting ZEB1 and ZEB2, ectopic expression of the miR-200s causes upregulation of E-cadherin and reduces cell motility[22–27,33,41]. The stress signature, defined by genes correlated with miR-200a expression, is the novel feature of our study. The fibrosis and stress signatures predict survival only when both are taken into account. Stratifying subjects with the fibrosis signature alone did not predict survival, further indicating that the stress component is a key effector of miR-200a and miR-141 in ovarian tumors. The miR-200s were shown to be highly expressed in localized tumors and downregulated in metastases, defining a two-stage model of miR-200 expression[48–50]. Our data are consistent with this model in two ways: we observed (i) a stage of high miR-200 expression, which provided a selective advantage to cancer cells but was associated with high sensitivity to treatment, in part by modulating the stress response, followed by (ii) a dissemination stage during which miR-200 expression was lost, further facilitating the spread of cancer cells and conferring resistance to chemotherapeutic agents. Consistent with our signatures, several studies have shown that high miR-200s expression is linked to a favorable prognosis[40,41,51], with downregulation of the miR-200s being associated with relapse in patients with ovarian cancer[52]. The segregation of high-grade ovarian carcinomas into miR-200a–dependent stress and fibrosis subgroups is associated with short- and long-term prognoses, specifically in regard to clinical response and disease progression. Our findings have broad implications for applications in clinical research. One could speculate that tumors with the stress pattern may be best treated with an optimal combination of ROS-producing chemotherapy and maximal surgery. In contrast, tumors with the fibrosis pattern, characterized by a low debulking efficiency and reduced treatment response, should be subjected to alternative approaches based on further molecular characterization. Future clinical trials may consider our results to generate prospective confirmation data. Such approaches could greatly enhance the multidisciplinary strategy currently applied in ovarian carcinomas.

In this paper we show a new mechanism of action for miR-141 and miR-200a in oxidative stress response by identifying p38α MAPK as one of their relevant targets. Alignments of *MAPK14* 3′ untranslated region sequences from various species indicate that Mpk2, the p38α homolog in *Drosophila*, is predicted to be a target of miR-8, the miR-141 and miR-200a ortholog[53–55]. Because miR-8 regulates the osmotic stress response, the crosstalk between miR-200, p38α and stress could be conserved through evolution. p38α MAPK was previously shown to reduce tumorigenesis by acting on cell proliferation, survival and stress response[14,15]. miRNA-dependent downregulation of p38α mimics the phenotype observed in p38α deficiency[10]. In addition, inactivation of p38α, either pharmacologically or genetically, is associated

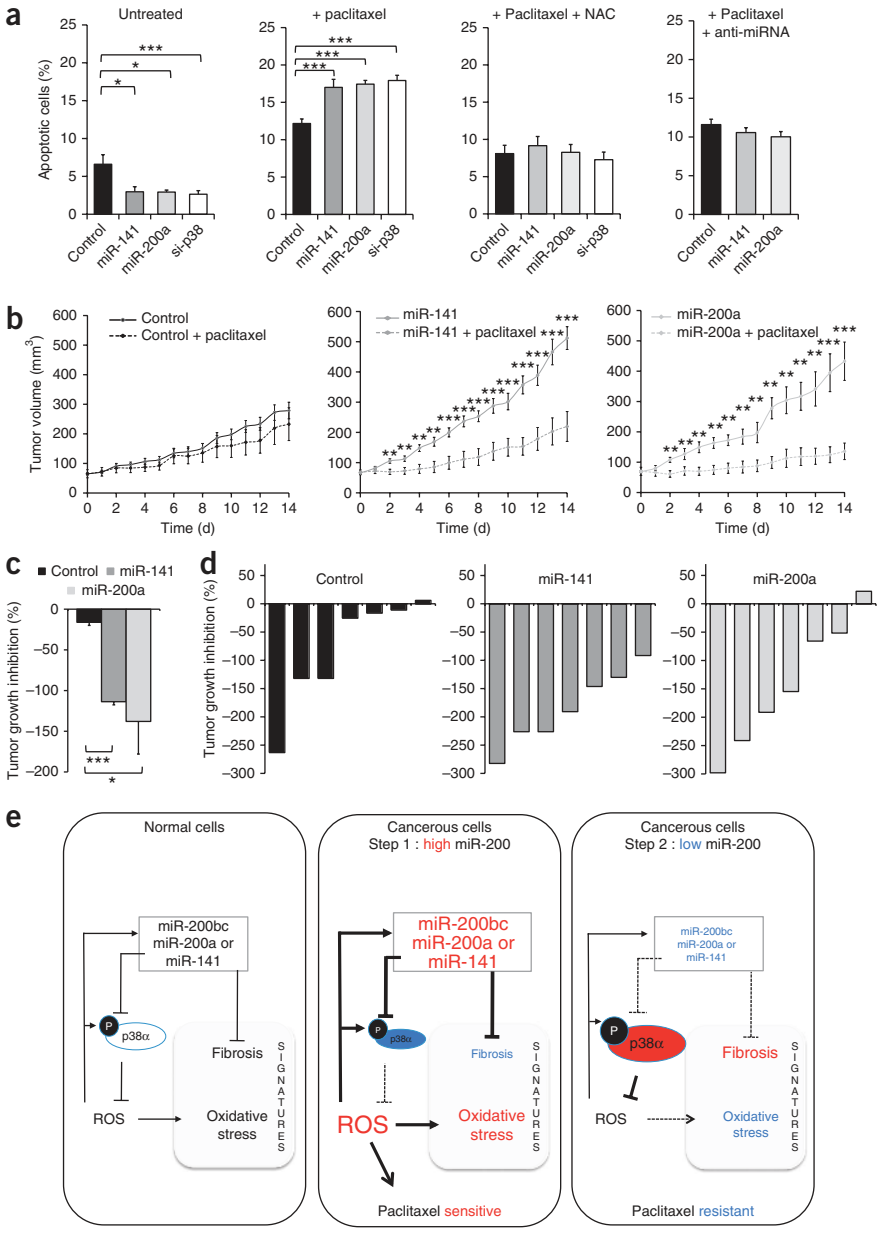

Figure 5 miR-141 and miR-200a enhance the response to chemotherapeutic reagents. (**a**) Histograms showing the percentage of apoptotic (annexin V positive and DAPI negative) SKOV3 cells transfected with miR-141, miR-200a or siRNA-p38 (si-p38) with or without treatment. NAC, *N*-acetylcysteine. (**b**) Growth curves of control, miR-141– or miR-200a–overexpressing tumors under untreated conditions (solid lines) or after treatment with paclitaxel (dashed lines). (**c**) Percentage of tumor growth inhibition after 8 d of treatment with paclitaxel. $n \geq 11$ tumors in each category for each condition (treated or untreated). (**d**) Percentage of tumor growth inhibition per tumor after 8 d of treatment with paclitaxel. (**e**) In normal cells (left), the reciprocal crosstalk between miR-141 or miR-200a, p38α and ROS allows for a mutual balance of each partner, further ensuring the integrity of the MAPK stress response pathways and low concentrations of ROS. In cancer cells, two successive stages can be considered, as has been previously stated[48–50]. At the early stage (middle), one can postulate that concentrations of ROS rise because, at least in part, of oncogenic transformation and metabolic alterations. High concentrations of ROS promote the accumulation of the miR-200s, which, in turn, reduce p38α. Chronically elevated ROS and miR-200s drive a persistent oxidative stress response, which is associated with an improved sensitivity to paclitaxel. At the advanced tumor stage (right), the downregulation of the miR-200s directly boosts p38α and ZEB1 or ZEB2 activity, thus restoring the normal stress response and inducing an epithelial-mesenchymal transition–like phenotype, which could be part of the fibrosis signature. Data are means ± s.e.m. $^{*}P \leq 0.05$, $^{**}P \leq 0.01$, $^{***}P \leq 0.001$ (Student's *t* test).

with ROS accumulation and the subsequent stimulation of antioxidant defenses mediated in part by Nrf2 (refs. 10,56). Nrf2-dependent genes are also markedly upregulated in ovarian tumors with high miR-200a expression and subsequent low amounts of p38α. miR-200a overexpression, as well as p38α inactivation, sensitizes ovarian cancer cells to paclitaxel, which is prevented with the use of antioxidants, further confirming the essential role of ROS in sensitivity to paclitaxel[34–36,57]. Recently published results showing that miR-200b, miR-200c and miR-429 target class III β-tubulin provided a molecular clue into the increased paclitaxel sensitivity in ovarian tumors overexpressing miR-200 (refs. 42,58). Our study provides new findings about other miR-200 family members, specifically miR-200a and miR-141, that increase paclitaxel sensitivity in an ROS-dependent manner by targeting p38α. To our knowledge, this is the first time that the effects of miR-141 and miR-200a have been shown on tumor growth and chemosensitivity using mouse models of ovarian cancer that corroborated human clinical data. Our results show a new function for miR-200 miRNAs and strengthen their direct implications in the antineoplastic effect of paclitaxel.

Our data indicate that oxidative stress has a dual role: it increases the growth rate of tumors and further promotes tumorigenesis, but it also potentiates the effect of ROS-producing therapeutic agents, for example, paclitaxel. These data may also provide new insights into clinical trials showing the lack of an obvious positive effect of antioxidant supplementation at pharmacological doses in the treatment of cancer. Conversely, it has been shown that cancer cells are very sensitive to ROS-producing agents, including piperlongumine[59]. The oxidative stress signature identified here could therefore be used as a predictive marker of response to treatment and survival. In conclusion, we identified a new reciprocal interaction between the miR-200s and the oxidative stress response that affects human ovarian carcinogenesis and prognosis.

METHODS

Methods and any associated references are available in the online version of the paper at http://www.nature.com/naturemedicine/.

Accession codes. The Institut Curie's ovarian cancer microarray data set is freely accessible in the Gene Expression Omibus under

the accession number GSE26193. H_2O_2-induced miRNA in the mouse fibroblast microarray data and data from fibroblasts overexpressing miR-141 or miR-200a are freely accessible in the Gene Expression Omnibus with the following accession numbers: GSE26194 and GSE26113.

Note: Supplementary information is available on the Nature Medicine website.

ACKNOWLEDGMENTS

We thank O. Delattre and S. Chanock for fruitful discussions and comments on the manuscript. We acknowledge S. Alran and B. Baranger (Surgery Department of Institut Curie) and the Biological Resource Center of Institut Curie for providing human ovarian tumors and B. Hasselain and D. Hajage for advice regarding our statistical analyses. We thank the members of the animal facility and the flow-cytometry platform of Institut Curie for their expertise. The experimental work was supported by grants from Institut National de la Santé et de la Recherche Médicale, the Institut Curie, the Ligue Nationale Contre le Cancer, the Institut National du Cancer and the Association pour la Recherche Contre le Cancer. B.M. was supported by a post-doctoral fellowship from the INSERM Avenir program and the Association pour la Recherche Contre le Cancer.

AUTHOR CONTRIBUTIONS

B.M. and F.M.-G. participated in the conception and design of the experiments. B.M., L.B., M.C., T.G. and Y.d.F. performed the experiments. X.S.-G. selected the human ovarian cancers after adapted characterization, and J.-P.M. provided transcriptome data. P.C. provided the associated clinical data from the subjects. O.M. and A.N. provided technical assistance and expertise in the ovarian tumor sample preparation. J.-P.M., B.M., L.B. and M.C. contributed to the statistical analyses of the data. F.M.-G. wrote the paper with suggestions and comments from all authors.

COMPETING FINANCIAL INTERESTS

The authors declare no competing financial interests.

Published online at http://www.nature.com/naturemedicine/.
Reprints and permissions information is available online at http://www.nature.com/reprints/index.html.

1. Hennessy, B.T., Coleman, R.L. & Markman, M. Ovarian cancer. *Lancet* **374**, 1371–1382 (2009).
2. The Cancer Genome Atlas Research Network. Integrated genomic analyses of ovarian carcinoma. *Nature* **474**, 609–615 (2011).
3. Allen, R.G. & Tresini, M. Oxidative stress and gene regulation. *Free Radic. Biol. Med.* **28**, 463–499 (2000).
4. Gerald, D. *et al.* JunD reduces tumor angiogenesis by protecting cells from oxidative stress. *Cell* **118**, 781–794 (2004).
5. Pouysségur, J. & Mechta-Grigoriou, F. Redox regulation of the hypoxia-inducible factor. *Biol. Chem.* **387**, 1337–1346 (2006).
6. Laurent, G. *et al.* Oxidative stress contributes to aging by enhancing pancreatic angiogenesis and insulin signaling. *Cell Metab.* **7**, 113–124 (2008).
7. Weinberg, F. & Chandel, N.S. Reactive oxygen species–dependent signaling regulates cancer. *Cell. Mol. Life Sci.* **66**, 3663–3673 (2009).
8. Pani, G., Galeotti, T. & Chiarugi, P. Metastasis: cancer cell's escape from oxidative stress. *Cancer Metastasis Rev.* **29**, 351–378 (2010).
9. Toullec, A. *et al.* Oxidative stress promotes myofibroblast differentiation and tumour spreading. *EMBO Mol. Med.* **2**, 211–230 (2010).
10. Dolado, I. *et al.* p38α MAP kinase as a sensor of reactive oxygen species in tumorigenesis. *Cancer Cell* **11**, 191–205 (2007).
11. Kennedy, N.J., Cellurale, C. & Davis, R.J. A radical role for p38 MAPK in tumor initiation. *Cancer Cell* **11**, 101–103 (2007).
12. Hui, L. *et al.* p38α suppresses normal and cancer cell proliferation by antagonizing the JNK-c-Jun pathway. *Nat. Genet.* **39**, 741–749 (2007).
13. Wada, T. *et al.* Antagonistic control of cell fates by JNK and p38-MAPK signaling. *Cell Death Differ.* **15**, 89–93 (2008).
14. Wagner, E.F. & Nebreda, A.R. Signal integration by JNK and p38 MAPK pathways in cancer development. *Nat. Rev. Cancer* **9**, 537–549 (2009).
15. Kim, E.K. & Choi, E.J. Pathological roles of MAPK signaling pathways in human diseases. *Biochim. Biophys. Acta* **1802**, 396–405 (2010).
16. Marsit, C.J., Eddy, K. & Kelsey, K.T. MicroRNA responses to cellular stress. *Cancer Res.* **66**, 10843–10848 (2006).
17. Ivan, M., Harris, A.L., Martelli, F. & Kulshreshtha, R. Hypoxia response and microRNAs: no longer two separate worlds. *J. Cell Mol. Med.* **12**, 1426–1431 (2008).
18. Lin, Y. *et al.* Involvement of microRNAs in hydrogen peroxide–mediated gene regulation and cellular injury response in vascular smooth muscle cells. *J. Biol. Chem.* **284**, 7903–7913 (2009).
19. Simone, N.L. *et al.* Ionizing radiation–induced oxidative stress alters miRNA expression. *PLoS ONE* **4**, e6377 (2009).
20. Wang, Z. *et al.* Profiles of oxidative stress–related microRNA and mRNA expression in auditory cells. *Brain Res.* **1346**, 14–25 (2010).
21. Magenta, A. *et al.* miR-200c is up-regulated by oxidative stress and induces endothelial cell apoptosis and senescence via ZEB1 inhibition. *Cell Death Differ.* **18**, 1628–1639 (2011).
22. Hurteau, G.J., Carlson, J.A., Spivack, S.D. & Brock, G.J. Overexpression of the microRNA hsa-miR-200c leads to reduced expression of transcription factor 8 and increased expression of E-cadherin. *Cancer Res.* **67**, 7972–7976 (2007).
23. Bracken, C.P. *et al.* A double-negative feedback loop between ZEB1–SIP1 and the microRNA-200 family regulates epithelial-mesenchymal transition. *Cancer Res.* **68**, 7846–7854 (2008).
24. Burk, U. *et al.* A reciprocal repression between ZEB1 and members of the miR-200 family promotes EMT and invasion in cancer cells. *EMBO Rep.* **9**, 582–589 (2008).
25. Gregory, P.A. *et al.* The miR-200 family and miR-205 regulate epithelial to mesenchymal transition by targeting ZEB1 and SIP1. *Nat. Cell Biol.* **10**, 593–601 (2008).
26. Korpal, M., Lee, E.S., Hu, G. & Kang, Y. The miR-200 family inhibits epithelial-mesenchymal transition and cancer cell migration by direct targeting of E-cadherin transcriptional repressors ZEB1 and ZEB2. *J. Biol. Chem.* **283**, 14910–14914 (2008).
27. Park, S.M., Gaur, A.B., Lengyel, E. & Peter, M.E. The miR-200 family determines the epithelial phenotype of cancer cells by targeting the E-cadherin repressors ZEB1 and ZEB2. *Genes Dev.* **22**, 894–907 (2008).
28. Shimono, Y. *et al.* Downregulation of miRNA-200c links breast cancer stem cells with normal stem cells. *Cell* **138**, 592–603 (2009).
29. Wellner, U. *et al.* The EMT-activator ZEB1 promotes tumorigenicity by repressing stemness-inhibiting microRNAs. *Nat. Cell Biol.* **11**, 1487–1495 (2009).
30. Iliopoulos, D. *et al.* Loss of miR-200 inhibition of Suz12 leads to polycomb-mediated repression required for the formation and maintenance of cancer stem cells. *Mol. Cell* **39**, 761–772 (2010).
31. Schickel, R., Park, S.M., Murmann, A.E. & Peter, M.E. miR-200c regulates induction of apoptosis through CD95 by targeting FAP-1. *Mol. Cell* **38**, 908–915 (2010).
32. Chang, C.J. *et al.* p53 regulates epithelial-mesenchymal transition and stem cell properties through modulating miRNAs. *Nat. Cell Biol.* **13**, 317–323 (2011).
33. Kim, T. *et al.* p53 regulates epithelial-mesenchymal transition through microRNAs targeting ZEB1 and ZEB2. *J. Exp. Med.* **208**, 875–883 (2011).
34. Ramanathan, B. *et al.* Resistance to paclitaxel is proportional to cellular total antioxidant capacity. *Cancer Res.* **65**, 8455–8460 (2005).
35. Alexandre, J., Hu, Y., Lu, W., Pelicano, H. & Huang, P. Novel action of paclitaxel against cancer cells: bystander effect mediated by reactive oxygen species. *Cancer Res.* **67**, 3512–3517 (2007).
36. Konstantinopoulos, P.A. *et al.* Carboplatin-induced gene expression changes *in vitro* are prognostic of survival in epithelial ovarian cancer. *BMC Med. Genomics* **1**, 59 (2008).
37. Liu, H. *et al.* mRNA and microRNA expression profiles of the NCI-60 integrated with drug activities. *Mol. Cancer Ther.* **9**, 1080–1091 (2010).
38. Iorio, M.V. *et al.* MicroRNA signatures in human ovarian cancer. *Cancer Res.* **67**, 8699–8707 (2007).
39. Nam, E.J. *et al.* MicroRNA expression profiles in serous ovarian carcinoma. *Clin. Cancer Res.* **14**, 2690–2695 (2008).
40. Hu, X. *et al.* A miR-200 microRNA cluster as prognostic marker in advanced ovarian cancer. *Gynecol. Oncol.* **114**, 457–464 (2009).
41. Bendoraite, A. *et al.* Regulation of miR-200 family microRNAs and ZEB transcription factors in ovarian cancer: evidence supporting a mesothelial-to-epithelial transition. *Gynecol. Oncol.* **116**, 117–125 (2010).
42. Cochrane, D.R., Howe, E.N., Spoelstra, N.S. & Richer, J.K. Loss of miR-200c: a marker of aggressiveness and chemoresistance in female reproductive cancers. *J. Oncol.* **2010**, 821717 (2010).
43. Mezzanzanica, D., Bagnoli, M., De Cecco, L., Valeri, B. & Canevari, S. Role of microRNAs in ovarian cancer pathogenesis and potential clinical implications. *Int. J. Biochem. Cell Biol.* **42**, 1262–1272 (2010).
44. van Jaarsveld, M.T., Helleman, J., Berns, E.M. & Wiemer, E.A. MicroRNAs in ovarian cancer biology and therapy resistance. *Int. J. Biochem. Cell Biol.* **42**, 1282–1290 (2010).
45. Tothill, R.W. *et al.* Novel molecular subtypes of serous and endometrioid ovarian cancer linked to clinical outcome. *Clin. Cancer Res.* **14**, 5198–5208 (2008).
46. Yang, H. *et al.* MicroRNA expression profiling in human ovarian cancer: miR-214 induces cell survival and cisplatin resistance by targeting PTEN. *Cancer Res.* **68**, 425–433 (2008).
47. Wyman, S.K. *et al.* Repertoire of microRNAs in epithelial ovarian cancer as determined by next generation sequencing of small RNA cDNA libraries. *PLoS ONE* **4**, e5311 (2009).
48. Olson, P. *et al.* MicroRNA dynamics in the stages of tumorigenesis correlate with hallmark capabilities of cancer. *Genes Dev.* **23**, 2152–2165 (2009).
49. Gibbons, D.L. *et al.* Contextual extracellular cues promote tumor cell EMT and metastasis by regulating miR-200 family expression. *Genes Dev.* **23**, 2140–2151 (2009).

50. Wiklund, E.D. *et al.* Coordinated epigenetic repression of the miR-200 family and miR-205 in invasive bladder cancer. *Int. J. Cancer* **128**, 1327–1334 (2011).
51. Eitan, R. *et al.* Tumor microRNA expression patterns associated with resistance to platinum based chemotherapy and survival in ovarian cancer patients. *Gynecol. Oncol.* **114**, 253–259 (2009).
52. Marchini, S. *et al.* Association between miR-200c and the survival of patients with stage I epithelial ovarian cancer: a retrospective study of two independent tumour tissue collections. *Lancet Oncol.* **12**, 273–285 (2011).
53. Karres, J.S., Hilgers, V., Carrera, I., Treisman, J. & Cohen, S.M. The conserved microRNA miR-8 tunes atrophin levels to prevent neurodegeneration in *Drosophila*. *Cell* **131**, 136–145 (2007).
54. Hyun, S. *et al.* Conserved MicroRNA miR-8/miR-200 and its target USH/FOG2 control growth by regulating PI3K. *Cell* **139**, 1096–1108 (2009).
55. Flynt, A.S. *et al.* miR-8 microRNAs regulate the response to osmotic stress in zebrafish embryos. *J. Cell Biol.* **185**, 115–127 (2009).
56. Naidu, S., Vijayan, V., Santoso, S., Kietzmann, T. & Immenschuh, S. Inhibition and genetic deficiency of p38 MAPK up-regulates heme oxygenase-1 gene expression via Nrf2. *J. Immunol.* **182**, 7048–7057 (2009).
57. Helleman, J., Smid, M., Jansen, M.P., van der Burg, M.E. & Berns, E.M. Pathway analysis of gene lists associated with platinum-based chemotherapy resistance in ovarian cancer: the big picture. *Gynecol. Oncol.* **117**, 170–176 (2010).
58. Leskelä, S. *et al.* The miR-200 family controls β-tubulin III expression and is associated with paclitaxel-based treatment response and progression-free survival in ovarian cancer patients. *Endocr. Relat. Cancer* **18**, 85–95 (2011).
59. Raj, L. *et al.* Selective killing of cancer cells by a small molecule targeting the stress response to ROS. *Nature* **475**, 231–234 (2011).

ONLINE METHODS

Ovarian cancer sample collection. Ovarian tumors were obtained from a cohort of patients treated at the Institut Curie between 1989 and 2005. The median age of the patients was 57.8 years (with a range of 31–86 years). Ovarian carcinomas were classified according to the World Health Organization histological classification of gynecological tumors. Pathological analysis identified 82 serous tumors, 8 mucinous tumors, 8 endometrioid tumors, 6 clear-cell carcinomas, 2 carcinosarcomas and 1 malignant Brenner tumor. One-hundred subjects were classified as having a high (grade 2 and 3) histological grade, and seven subjects were classified as having a low (grade 1) histological grade. Thirty-one subjects (29%) were considered to be in the early stages (International Federation of Gynecology and Obstetrics (FIGO) I–IIc) and 76 subjects (71%) were considered to be in an advanced stage (III or IV) of disease. Patients were treated with a combination of surgery and chemotherapy, the latter of which included alkylating or alkylating-like agents with or without taxane as a first-line treatment. The study was approved by the Institutional Review Board and Ethics committee of the Institut Curie. Before inclusion in the study, patients were informed that their biological samples could be used for research purposes and that they had the right to refuse if they so wished. Analysis of tumor samples was performed according to the relevant national law on the protection of people taking part in biomedical research.

qRT-PCR of mRNA and miRNA in ovarian tumors and cell lines. For the mRNA analysis, 1 μg of total RNA was reverse transcribed using an iScript Reverse Transcription Kit (Bio-Rad), and qRT-PCR was performed using Power SYBR Green PCR Master Mix (Applied Biosystems) on a Chromo4 System (Bio-Rad). Data were analyzed using an Opticon Monitor (Bio-Rad) and normalized to GAPDH mRNA (cell lines) or to the average of hypoxanthine guanine phosphoribosyl transferase (HPRT), Ribosomal protein large P0 (RPLP0), glyceraldhyde-3-phosphate dehydrogenase (GAPDH) and β-2 microglobulin (B2M) mRNA levels (ovarian tumors) (see **Supplementary Table 6** for sequences). Mature miRNA levels were quantified using TaqMan miRNA Assays (Applied Biosystems) and normalized to the average of U6 small nucleolar RNA and miR-16 (cell lines) or to the average of U6B, U6, RNU24, RNU49 and RNU48 small RNA levels (ovarian tumors); fold changes were calculated using the $2^{-\Delta\Delta Ct}$ method. Relative miR-200a and miR-141 levels were quantified from RNA from a subset of 82 ovarian tumors.

Ovarian microarray data sets and gene expression profiling. Ovarian tumor samples were analyzed on a Human Genome U133 Plus 2.0 array (Affymetrix) according to the manufacturer's procedures[60]. Transcriptome data were normalized using the Guanine Cytosine Robust Multiarray Analysis (GCRMA) algorithm. Only probes with a log intensity value greater than 3.5 (log2) in at least 80% of the samples were kept for further analysis. The microarray normalization and analysis were performed using Partek Genomic Suite software (Partek). The dataset from the Institute Curie, from which we determined miR-200a expression values, the correlation between mature miR-200a levels and the detected probe sets, was calculated using a Pearson correlation coefficient. The probe sets, identified as either positively or negatively correlated with miR-200a, were submitted to analysis using IPA software. Enriched canonical pathways were selected using a Fisher exact test, and adjusted *P* values ($P \leq 0.05$) were calculated using a Benjamini-Hochberg multiple-testing correction. For the probe sets that were correlated with miR-200a, the most significant Ingenuity canonical pathway was "Nrf2-mediated oxidative stress response," and for probe sets anticorrelated with miR-200a, the most significant Ingenuity canonical pathway was "Hepatic fibrosis–hepatic stellate cell activation." Genes composing the stress and fibrosis signatures are listed in **Supplementary Table 4**.

Immunohistochemistry from human ovarian carcinomas. A tissue microarray from 56 ovarian serous adenocarcinomas was created using two cores of tumor tissue per subject (each 1 mm in diameter) hybridized simultaneously. Sections of paraffin-embedded tissue (3 μm) were stained using the streptavidin-peroxidase protocol (Benchmark Immunostainer, Ventana) with specific antibodies recognizing p38α (1:50 dilution; 9218, Cell Signaling). For quantification, two sections from distinct areas of each tumor were evaluated independently by two different investigators. An immunohistochemistry score (ranging from 0 to 4) was calculated as follows: (staining intensity × percentage of positively labeled cells)/100.

miRNA microarray data from mouse fibroblasts and fibroblasts overexpressing miR-141 or miR-200a. The methods used for this analysis are described in the **Supplementary Methods**.

Xenograft experiments. The cell lines and antibodies used in these experiments are described in the **Supplementary Methods**. Graft experiments were performed by subcutaneous injection of 2×10^5 fibroblasts or 3×10^6 exponentially growing SKOV3 cells into 6-week-old nude female mice. The mice were checked daily for tumor growth using calipers. Tumor volume was determined using the following equation: $0.5 \times (\text{length} \times \text{width}^2)$. When tumors reached a volume of 75 mm^3, paclitaxel treatment was triggered using a single intraperitoneal injection of paclitaxel (Hospira) at 30 mg per kg of body weight. The percentage of tumor growth inhibition was calculated using the following formula: $100 - 100 \times$ (tumor volume from untreated mice/tumor volume from paclitaxel-treated mice). The Institut Curie's ethical committee approved all mouse experiments.

Apoptosis assays. Apoptosis was monitored by annexin V (561012, BD Biosciences) and DAPI (1 μg ml^{-1}) staining according to the manufacturer's instructions. Where indicated, cells were treated with 20 nM paclitaxel for 48 h and with 4 mM NAC daily. Apoptotic cells were defined as the population that was positive for annexin and negative for DAPI. FACS experiments were conducted on an LSRII cytometer, and data were analyzed using FlowJo 9.1 software.

Statistical analyses. All experiments were performed in triplicate, and data shown are means ± s.e.m. (unless otherwise specified) from at least three independent experiments. Differences were considered to be statistically significant at values of $P \leq 0.05$ by Student's *t* test or Mann-Whitney test. Single, double and triple asterisks indicate statistically significant differences: $^*P \leq 0.05$; $^{**}P \leq 0.01$; $^{***}P \leq 0.001$. All survival analyses were carried out using Kaplan-Meier method and log-rank test in R. Univariate or multivariate Cox proportional hazards regression was conducted with SPSS 19.0 software using the enter method.

60. Meyniel, J.P. *et al.* A genomic and transcriptomic approach for a differential diagnosis between primary and secondary ovarian carcinomas in patients with a previous history of breast cancer. *BMC Cancer* **10**, 222 (2010).

doi:10.1038/nm.2512